

[Supporting Information]

Real Time Kinetics of Surfactant Molecules Transfer between Emulsion Particles Probed by *In Situ* Second Harmonic Generation Spectroscopy

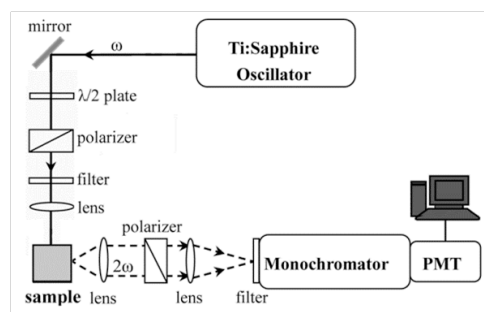
YuMeng You, Aaron Bloomfield, Jian Liu, Li Fu, Seth B. Herzon*, and Elsa C. Y. Yan*
Department of Chemistry, Yale University, 225 Prospect Street, New Haven, CT 06520

CONTENT:

- A. Second Harmonic Generation (SHG) Setup
- B. Preparation of Emulsion
- C. Synthesis Processes of MG-butyl-1 and MG-octyl-1
- D. Adsorption Isotherm
- E. UV-visible Absorption of Emulsion Particles
- F. Stability of Donor and Acceptor Particles
- G. Characterization Spectra of Novel Compounds
- H. Theoretical Background of SHG: Probing Surfaces of Micron-Sized Colloidal Particles
- I. Experimental Evidence of the ρN^2 Dependence of I_{SHG}

A. Second Harmonic Generation (SHG) Setup

The SHG setup (Scheme S1) contains a Ti:sapphire oscillator (Mai Tai XF, Spectra-Physics), which provides 120 fs pulses at 800 nm with a repetition rate of 80 MHz. In the SHG experiments, the fundamental light was focused into a 1-cm quartz cuvette, and the SHG signal at 400 nm were detected at 90° with respect to incident laser beam. The spot size of the fundamental beam is 50 μm in diameter and the focal volume is $2.5 \times 10^6 \mu\text{m}^3$. The signal was spectrally dispersed by a monochromator (Acton SP2150, Princeton Instruments) and then detected by a PMT (R4220P, Hamamatsu) connected to a single-photon-counting system (SR400, SRS).



Scheme S1. SHG setup

B. Preparation of Emulsion

A volume of 1 mL 5 mM 1-dodecanol (Aldrich, > 99%)/n-tetradecane (Aldrich, > 99%) was first mixed with 9 mL 5 mM sodium dodecyl sulfate (SDS) (Sigma, > 99%)/water solution in a 16 x 100 mm test tube. The refractive indices of the oil phase and water phase are 1.43 and 1.33. The mixture was

ultrasonicated (QSONICA) using a titanium probe (3.2 mm in diameter) on ice. To avoid heating, ultrasonication was paused for 30 s after every 60 s operation, and such a cycle was repeated six times to yield homogenized emulsion.

C. Syntheses of MG-butyl-1 (2) and MG-octyl-1 (3):

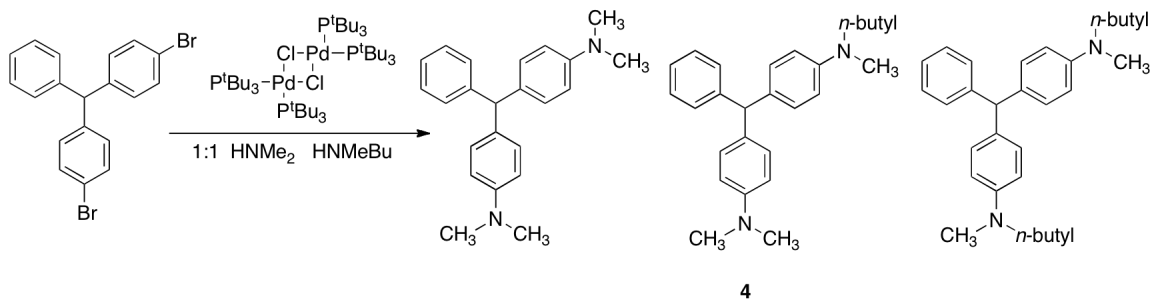
General Experimental Procedures. All reactions were performed in 1-dram vials, each fitted with a Teflon-lined screw cap (13-mm diameter, 425 GPI thread; supplied by Qorpak, Bridgeville, Pennsylvania) under an atmosphere of nitrogen, unless otherwise noted. Air- and moisture-sensitive reagents were handled in a nitrogen-filled drybox (working oxygen level <5 ppm). Organic solutions were concentrated by rotary evaporation at 30–33 °C. Flash-column chromatography was performed as described by Still et al.,¹ employing silica gel (60 Å, 40–63 µm particle size) purchased from Silicycle (Quebec, Canada). Analytical thin-layered chromatography (TLC) was performed using glass plates pre-coated with silica gel (250 µm, 60 Å pore size) impregnated with a fluorescent indicator (254 nm). TLC plates were visualized by exposure to ultraviolet light (UV).

Materials. Commercial solvents and reagents were used as received with the following exceptions. Tetrahydrofuran was distilled from sodium–benzophenone immediately before use. Triethylamine was distilled from calcium hydride immediately before use.

Instrumentation. Proton nuclear magnetic resonance spectra (¹H NMR) were recorded at 400 or 500 MHz at 24 °C, unless otherwise noted. Chemical shifts are expressed in parts per million (ppm, δ scale) downfield from tetramethylsilane, and are referenced to residual protium in the NMR solvent (CHCl₃, δ 7.26; C₆D₆, δ 7.15). Data are represented as follows: chemical shift, multiplicity (s = singlet, d = doublet, t = triplet, q = quartet, quint = quintet, m = multiplet and/or multiple resonances, br = broad, app = apparent), integration, coupling constant in Hertz, and assignment. Proton-decoupled carbon nuclear magnetic resonance spectra (¹³C NMR) were recorded at 100 or 125 MHz at 24 °C, unless otherwise noted. Chemical shifts are expressed in parts per million (ppm, δ scale) downfield from tetramethylsilane, and are referenced to the carbon resonances of the solvent (CDCl₃, δ 77.0; C₆D₆, δ 128.0). Data are represented as follows: chemical shift, multiplicity (s = singlet, d = doublet, t = triplet, m = multiplet and/or multiple resonances, app = apparent), coupling constant in Hertz. Attenuated total reflectance Fourier transform infrared (ATR-FTIR) spectra were obtained using a Thermo Electron Corporation Nicolet 6700 FTIR spectrometer referenced to a polystyrene standard. Data are represented as follows: frequency of absorption (cm⁻¹), intensity of absorption (s = strong, m = medium, w = weak, br = broad, assignment). High-resolution mass spectrometry (HRMS) data was obtained on a Waters analytical ultra high-performance liquid chromatography-mass spectrometry (UPLC/HRMS) instrument equipped with an electrospray (ESI) mass spectrometry detector and photodiode array detector. Unless otherwise noted,

samples were eluted over a reverse-phase C18 column (1.7 μm particle size, 2.1 \times 50 mm) with a linear gradient of 5% acetonitrile–water to 95% acetonitrile–water containing 0.1% formic acid over 3 min at a flow rate of 0.8 mL/min.

Synthesis of MG-butyl-1 (2):

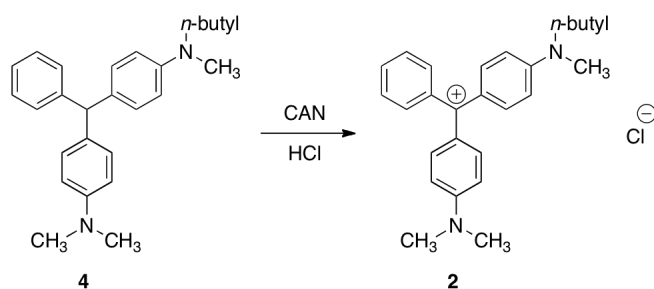


Step 1: Synthesis of 4-dimethylamino-4'-methyl-butylamino-triphenylmethane (4):

In a nitrogen-filled drybox, *N*-methyl-butylamine (7.0 μL , 58.6 μmol , 1.45 equiv) and a solution of dimethylamine in tetrahydrofuran (2.0 M, 25.0 μL , 50.0 μmol , 1.25 equiv) were added to a neat mixture of 4,4'-dibromo-triphenylmethane (16.4 mg, 40.8 μmol , 1 equiv), and sodium *tert*-butoxide (11.6 mg, 121 μmol , 2.96 equiv). A solution of μ -dibromo-tetrakis(tri-*tert*-butylphosphine)dipalladium in tetrahydrofuran (2.4 mM, 70.0 μL , 1.68 μmol , 0.41 mol%) was added to the mixture, and the resulting solution was stirred for 20 min at 24 $^{\circ}\text{C}$. The product mixture was diluted with distilled water (1.0 mL), and the diluted mixture was extracted with dichloromethane (3 \times 1.0 mL). The organic phases were combined, and the combined organic phases were dried over sodium sulfate. The dried solution was filtered, and the filtrate was concentrated. The residue obtained was purified by flash-column chromatography (eluting with 5% ethyl acetate–hexanes) with protection from light to afford separately 4-dimethylamino-4'-methyl-butylamino-triphenylmethane (**4**, 5.4 mg, 36%), 4,4'-bis(dimethylamino)-triphenylmethane (1.7 mg, 13%), and 4,4'-bis(methyl-butylamino)-triphenylmethane (5.8 mg, 34%) as clear, colorless oils.

Spectral data for **4**:

^1H NMR (400 MHz, C_6D_6) δ 7.35–7.31 (m, 2H), 7.23–7.17 (m, 6H), 7.08 (tt, $J_{\text{HH}} = 7.4$ Hz, $J_{\text{HH}} = 1.4$ Hz, 1H), 6.64–6.58 (m, 4H), 5.50 (s, 1H), 3.02 (t, $J_{\text{HH}} = 7.4$ Hz, 2H), 2.58 (s, 3H), 3.52 (s, 6H), 1.38–1.27 (m, 2H), 1.11 (sex, $J_{\text{HH}} = 7.6$ Hz, 2H), 0.78 (t, $J_{\text{HH}} = 7.4$ Hz, 3H). ^{13}C NMR (400 MHz, C_6D_6) δ 149.5 (C), 148.2 (C), 146.4 (C), 133.6 (C), 132.8 (C), 130.6 (CH), 130.5 (CH), 130.0 (CH), 128.4 (CH), 126.1 (CH), 113.2 (CH), 112.6 (CH), 55.8 (CH), 52.8 (CH_2), 40.5 (CH_3), 38.3 (CH_3), 29.2 (CH_2), 20.6 (CH_2), 14.1 (CH_3). IR (thin film), cm^{-1} : 2923.7 (m), 2853.2 (m), 1610.9 (m), 1515.0 (s), 1346.2 (m). LC/HRMS-ESI (m/z): $[\text{M} + \text{H}]^+$ calcd for $\text{C}_{26}\text{H}_{32}\text{N}_2$, 373.2644; found 373.2513.



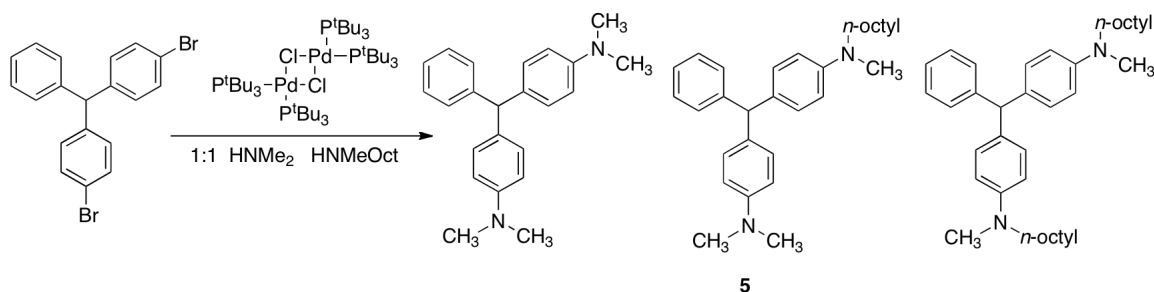
Step 2: Oxidation of 4-Dimethylamino-4'-methyl-butylamino-triphenylmethane:

4-Dimethylamino-4'-methylbutylamino-triphenylmethane (**4**, 5.4 mg, 14.5 μmol) was dissolved in tetrahydrofuran (1.0 mL). In a separate vessel, a solution of cerium (IV) ammonium nitrate (301 mg, 547 μmol) and 36% aqueous hydrochloric acid (50 μL , 583 μmol) in water (5.0 mL) was prepared. An aliquot of this solution (265 μL , 2.0 equiv ceric ammonium nitrate) was then added dropwise over 20 min via syringe to the diamine solution. The resulting dark blue product solution was diluted with water (5.0 mL). The diluted solution was extracted with ethyl acetate (5×15 mL). The organic phases were combined and the combined organic layers were dried over sodium sulfate. The dried solution was filtered and the filtrate was concentrated to afford MG-butyl-1 (**2**) as a dark blue solid (6.3 mg, 100%).

Spectral Data for MG-butyl-1 (**2**):

^1H NMR (500 MHz, CDCl_3) δ 7.69 (t, $J_{\text{HH}} = 8.0$ Hz, 1H), 7.54 (t, $J_{\text{HH}} = 7.5$ Hz, 2H), 7.40 (d, $J_{\text{HH}} = 8.5$ Hz, 3H), 7.34 (d, $J_{\text{HH}} = 7.0$ Hz, 2H), 6.96 (t, $J_{\text{HH}} = 10.5$ Hz, 3H), 3.62 (t, $J_{\text{HH}} = 7.5$ Hz, 2H), 3.63 (s, 6H), 3.33 (s, 3H), 1.74–1.66 (m, 2H), 1.45–1.39 (m, 2H), 0.99 (t, $J_{\text{HH}} = 7.5$ Hz, 3H). ^{13}C NMR (400 MHz, CDCl_3) δ 177.3 (C⁺), 157.1 (C), 156.5 (C), 141.3 (CH), 141.0 (CH), 139.7 (C), 134.8 (CH), 133.1 (CH), 128.7 (CH), 127.8 (C), 127.5 (C), 114.0 (CH), 113.9 (CH), 53.4 (CH₂), 41.2 (CH₃), 39.9 (CH₃), 29.6 (CH₂), 20.3 (CH₂), 14.0 (CH₃). IR (thin film), cm^{-1} : 2955.5 (w), 2929.8 (w), 2870.1 (w), 1610.7 (m), 1514.7 (s), 1346.1 (m). LC/HRMS-ESI (m/z): $[\text{M}]^+$ calcd for $\text{C}_{326}\text{H}_{31}\text{N}_2$, 371.2487; found 371.2339.

Synthesis of MG-octyl-1 (3**):**

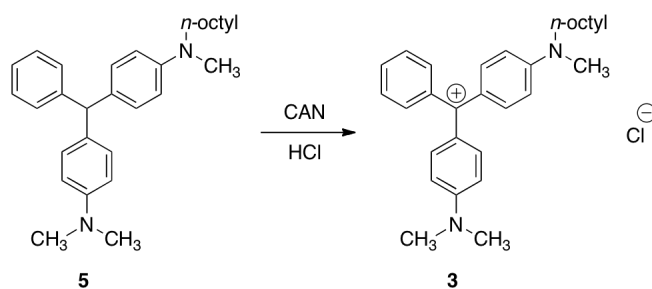


Step 1: Synthesis of 4-dimethylamino-4'-methyloctylamino-triphenylmethane (5):

In a nitrogen-filled glovebox, methyloctylamine (10 μL , 55.2 μmol , 1 equiv) and a 2.0 M solution of dimethylamine in tetrahydrofuran (30 μL , 60.0 μmol , 1.09 equiv) were added to a neat mixture of 4,4'-dibromo-triphenylmethane (23.6 mg, 58.7 μmol , 1 equiv), and sodium *tert*-butoxide (16.2 mg, 169 μmol , 2.9 equiv). A 2.4 mM solution of μ -dibromo-tetrakis(tri-*tert*-butylphosphine)dipalladium in tetrahydrofuran (2.4 mM, 90.0 μL , 2.16 μmol , 0.38 mol%) was added to the mixture, and the resulting solution was stirred for 20 min at 24 $^{\circ}\text{C}$. The product mixture was diluted with deionized water (1.0 mL), and the diluted mixture was extracted with dichloromethane (3×1.0 mL). The organic phases were combined, and the combined organic phases were dried over sodium sulfate. The dried solution was filtered, and the filtrate was concentrated. The residue obtained was purified by flash-column chromatography (eluting with 5% ethyl acetate-hexanes) with protection from light to afford separately 4-dimethylamino-4'-methyloctylamino-triphenylmethane (**5**, 9.7 mg, 41%), 4,4'-bis(dimethylamino)-triphenylmethane (3.8 mg, 21%), and 4,4'-bis(methyloctylamino)-triphenylmethane (8.1 mg, 28%) as clear, colorless oils.

Spectral Data for 5:

^1H NMR (500 MHz, C_6D_6) δ 7.33 (d, $J_{\text{HH}} = 7.5$ Hz, 2H), 7.23–7.15 (m, 6H), 7.08 (t, $J_{\text{HH}} = 7.3$ Hz, 1H), 6.67–6.59 (m, 4H), 5.55 (s, 1H), 3.06 (t, $J_{\text{HH}} = 7.3$ Hz, 2H), 2.61 (s, 3H), 2.52 (s, 6H), 1.41 (quin, $J_{\text{HH}} = 6.8$ Hz, 2H), 1.32–1.09 (m, 12H), 0.91 (t, $J_{\text{HH}} = 7.0$ Hz, 3H). ^{13}C NMR (400 MHz, C_6D_6) δ 149.5 (C), 148.3 (C), 146.4 (C), 133.6 (C), 132.9 (C), 130.7 (CH), 130.5 (CH), 130.0 (CH), 128.4 (CH), 126.1 (CH), 113.2 (CH), 112.7 (CH), 55.8 (CH), 53.1 (CH_2), 40.5 (CH_3), 38.3 (CH_3), 32.3 (CH_2), 29.9 (CH_2), 29.8 (CH_2), 27.5 (CH_2), 27.1 (CH_2), 23.1 (CH_2), 14.4 (CH_3). IR (thin film), cm^{-1} : 2923.0 (m), 2852.8 (w), 1614.5 (w), 1579.1 (s), 1353.5 (s), 1167.9 (s). LC/HRMS-ESI (m/z): $[\text{M} + \text{H}]^+$ calcd for $\text{C}_{30}\text{H}_{40}\text{N}_2$, 429.3270; found 429.3063.



Step 2: Oxidation of 4-Dimethylamino-4'-methyloctylamino-triphenylmethane (5):

4-Dimethylamino-4'-methyloctylamino-triphenylmethane (**5**, 9.7 mg, 22.6 μmol) was dissolved in 1.0 mL tetrahydrofuran. Cerium (IV) ammonium nitrate (311 mg, 568 μmol) and concentrated hydrochloric acid (36%) (50 μL , 583 μmol) were dissolved in water (5.0 mL). The acidic solution of ceric ammonium nitrate (400 μL , 2.0 equiv CAN) was added dropwise over to the diamine solution over the

course of 20 min, affording a dark blue solution. The product mixture was diluted with water (5.0 mL) and the diluted solution was extracted with ethyl acetate (5 × 15 mL). The organic phases were combined, and the combined organic phases were dried over sodium sulfate. The dried solution was filtered and the filtrate was concentrated to afford the dye as a dark blue solid (8 mg, 77%).

Spectral Data for MG-octyl-1 (**3**):

¹H NMR (400 MHz, C₆D₆) δ 7.61 (d, *J*_{HH} = 7.6 Hz, 2H), 7.40 (d, *J*_{HH} = 8.8 Hz, 2H), 7.39 (d, *J*_{HH} = 8.8 Hz, 2H), 7.22–7.18 (m, 2H), 7.09 (tt, *J*_{HH} = 7.2 Hz, *J*_{HH} = 1.2 Hz, 1H), 6.60 (d, *J*_{HH} = 8.8 Hz, 2H), 6.55 (d, *J*_{HH} = 8.8 Hz, 2H), 3.05 (t, *J*_{HH} = 7.2 Hz, 2H), 2.59 (s, 3H), 2.50 (s, 6H), 1.42–1.38 (m, 2H), 1.05–1.33 (br, 10H), 0.91 (t, *J*_{HH} = 6.8 Hz, 3H). ¹³C NMR (400 MHz, CDCl₃) δ 177.3 (C+), 157.1 (C), 156.5 (C), 141.3 (CH), 141.1 (CH), 139.7 (C), 128.7 (CH), 127.8 (C), 127.5 (C), 114.0 (CH), 113.9 (CH), 53.7 (CH₂), 41.1 (CH₃), 39.7 (CH₃), 31.9 (CH₂), 29.5 (CH₂), 29.3 (CH₂), 27.6 (CH₂), 27.1 (CH₂), 22.8 (CH₂), 14.2 (CH₃). IR (thin film), cm⁻¹: 2957.0 (w), 2928.9 (w), 2870.8 (w), 1615.0 (w), 1578.6 (s), 1336.4 (s), 1164.6 (s). LC/HRMS-ESI (*m/z*): [M]⁺ calcd for C₃₀H₃₉N₂, 427.3113; found 427.2945.

D. Adsorption Isotherm

The adsorption isotherms of MG, MG-butyl-1 (**2**), and MG-octyl-1 (**3**) onto the emulsion particles were obtained. The particle density was kept constant (1.3×10^{10} particles/cm³), while the concentrations of MG, MG-butyl-1 (**2**), and MG-octyl-1 (**3**) were varied in the range of 0.5-8.0 μM . The SHG intensity of the samples was measured using an integration time of 2 sec and averaged over 40 sec. The UV-visible spectrum of each sample was obtained before and after the SHG measurements to ensure sample stability. The UV-visible measurements suggest that when the concentration of MG-butyl-1 (**2**) and MG-octyl-1(**3**) was higher than 3.7 μM and 2.7 μM , respectively, the emulsion system became unstable. Hence, the concentrations in the adsorption isotherm were kept below these limiting values.

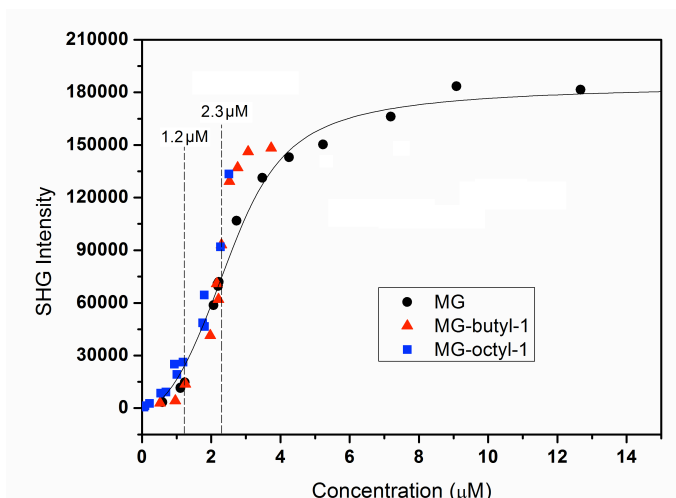


Figure S1. Adsorption isotherm for MG, MG-butyl-1 (**2**) and MG-octyl-1 (**3**) on the surface of emulsion. The solid line indicates the fitting curve for MG; the dashed lines indicate the concentrations used in the kinetic experiments.

Figure S1 shows the adsorption isotherm of MG (**1**), MG-butyl-1 (**2**), and MG-octyl-1 (**3**) onto the emulsion particles. At low concentration ($< 2.5 \mu\text{M}$), the MG (**1**), MG-butyl-1 (**2**), and MG-octyl-1 (**3**) isotherms exhibit similar isotherm. In our experiments, we chose the S_p concentration at 2.3 μM at $t < 0$ and 1.2 μM at $t > 0$. The adsorption isotherms show that these concentrations (dashed line in Figure S1) are below the saturation value. The emulsion system is stable even at high concentration of MG. Thus, adsorption saturation can be reached for MG (**1**). The adsorption isotherm of MG (**1**) is fitted into the following equation:^{2,3}

$$\frac{N}{N_{max}} = \frac{(C + N_{max} + 55.5/K_{eq}) - \sqrt{(C + N_{max} + 55.5/K_{eq})^2 - 4CN_{max}}}{2N_{max}} \quad (1),$$

where C is the total concentration of S_p , N_{max} is the maximum number of S_p adsorbing onto the surface of emulsion, K_{eq} is the equilibrium constant for the adsorption process. The fitting yields $N_{max} = 3.1 \pm 0.2$

μM and $K_{eq} = 4.1 \times 10^8 \text{ M}^{-1}$ for MG (**1**), in agreement with previous studies.³ The adsorption free energy is calculated from K_{eq} to be $-48 \text{ kJ}\cdot\text{M}^{-1}$ for MG (**1**). On the basis that each carbon on an alkyl chain contributes extra $\sim 5 \text{ kJ}\cdot\text{M}^{-1}$ to the adsorption free energy from an aqueous phase to an oil phase,⁴ we estimate that the adsorption free energy is $-63 \text{ kJ}\cdot\text{M}^{-1}$ for MG-butyl-1 (**2**) and $-83 \text{ kJ}\cdot\text{M}^{-1}$ for MG-octyl-1 (**3**), corresponding to $1/K_{eq}$ in the pico-molar and femto-molar range: $\sim 5.9 \times 10^{-12} \text{ M}$ for MG-butyl-1 (**2**) and $1/K_{eq} \sim 1.6 \times 10^{-15} \text{ M}$ for MG-octyl-1 (**3**). The adsorption isotherm for MG-butyl-1 (**2**) is fitted to yield $N_{max} = 3.0 \pm 0.1 \mu\text{M}$. However, K_{eq} cannot be obtained reliably from the fitting mostly because the experimental concentration range ($0.5\text{-}8.0 \mu\text{M}$) was orders of magnitudes higher than $1/K_{eq}$. The fitted N_{max} are the same for MG and MG-butyl-1. Hence, N_{max} is likely to be determined by the size of the MG head group. We assume that MG-octyl-1 has a similar $N_{max} \sim 3.0 \mu\text{M}$. Using the estimated values of K_{eq} and N_{max} , we calculated the concentration of *Sp* remaining in bulk solution for MG-butyl-1 (**2**) and MG-octyl-1 (**3**) under our experimental condition at a total *Sp* concentration of $1.2 \mu\text{M}$. We found that the bulk *Sp* concentration is 2×10^{-4} for MG-butyl-1 (**2**) and $6 \times 10^{-8} \mu\text{M}$ for MG-octyl-1 (**3**), accounting for less than 1% of the total *Sp* concentration.

E. UV-visible Absorption of Emulsion Particles

The emulsion was diluted to various concentrations and UV-visible spectroscopy was used to characterize and monitor the stability of the solution. In Figure S2, the optical density at different wavelength was plotted against the emulsion particle density. A linear dependence was obtained at various wavelength, indicating the emulsion remains stable upon dilution.

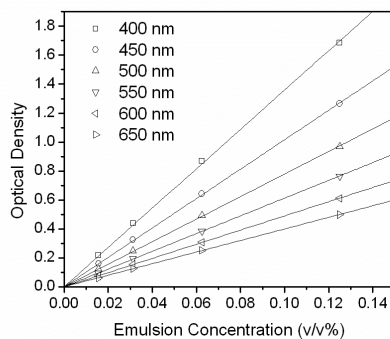


Figure. S2. Dependence of optical density on emulsion particle density at various wavelengths. The straight lines are linear fit of the experimental data.

F. Stability of Donor and Acceptor Particles

UV-visible spectra of acceptor particle (AP) and donor particles (DP) containing MG-butyl-1 (**2**) and MG (**1**) were also collected before the SHG measurements (Fig. S3). The spectra of AP show only a

scattering background of the emulsion particles. This background does not change upon addition of MG-Octyl-1 (**3**), MG-butyl-1 (**2**) and MG (**1**), leading to the conclusion that the emulsion system was still stable in the presence of surfactant probe molecules. This UV-visible characterization was repeated after the SHG measurements. The scattering background also remains the same, suggestion that the emulsion system was stable during the SHG experiments.

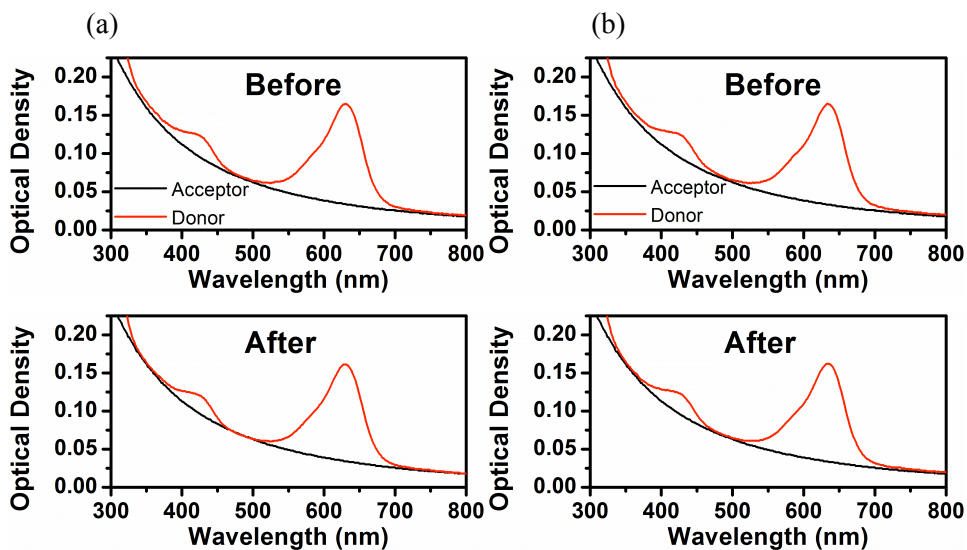
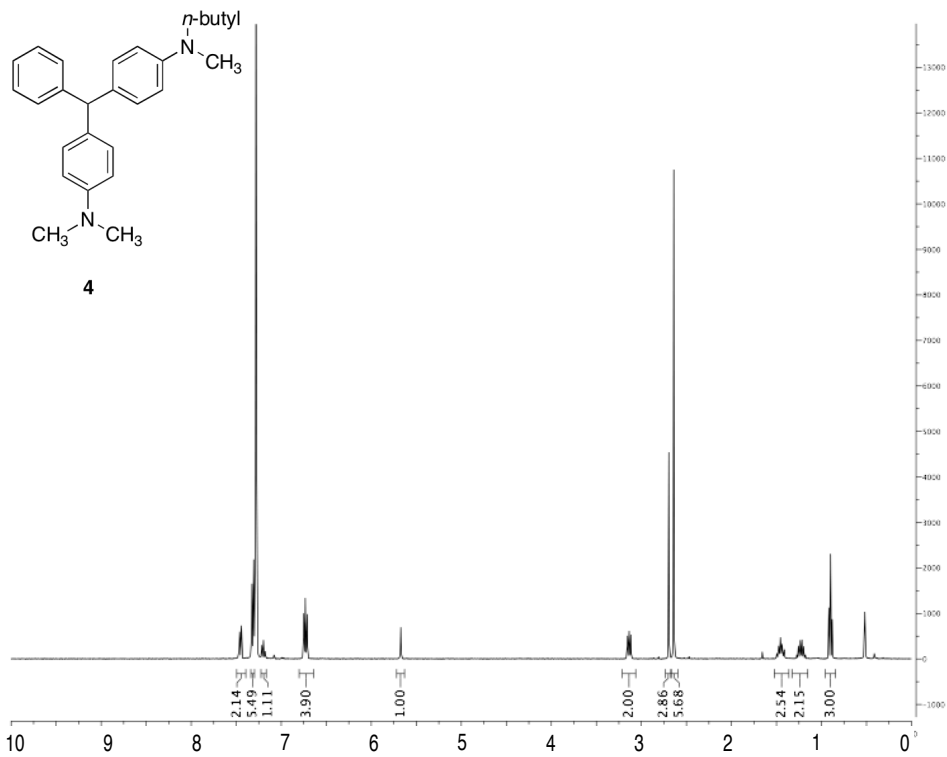


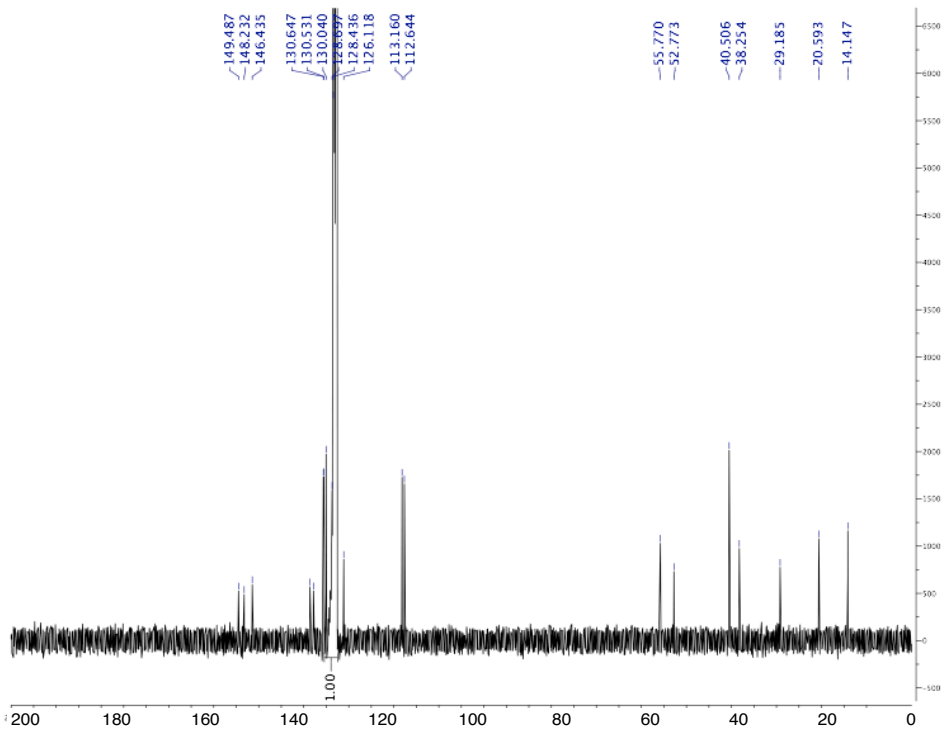
Figure S3. The UV-visible absorption spectra of donor particle (red) and acceptor particles (black) for (a) MG and (b) MG-butyl-1. Emulsion particle density was 1.3×10^{10} particle/cm³, and concentrations of surfactant probe molecules were $2.3 \mu\text{M}$.

G. Characterization Spectra of Novel Compounds

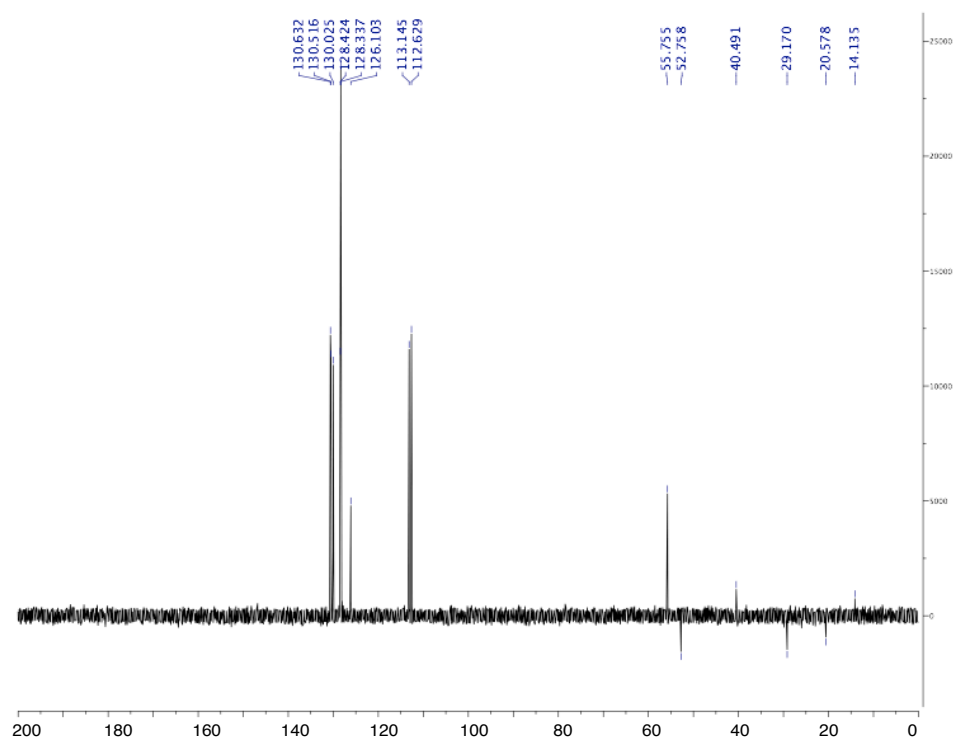
^1H NMR



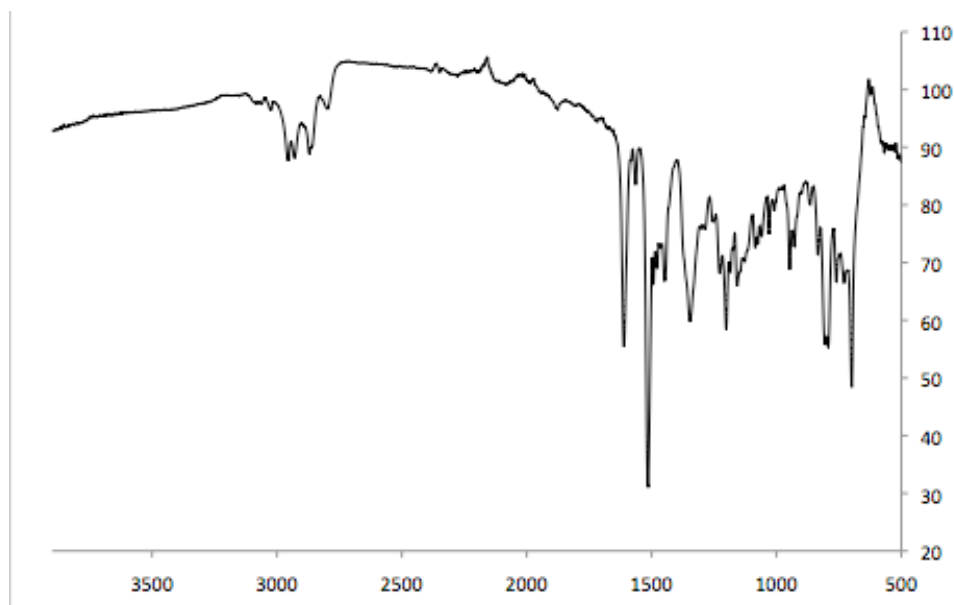
^{13}C NMR



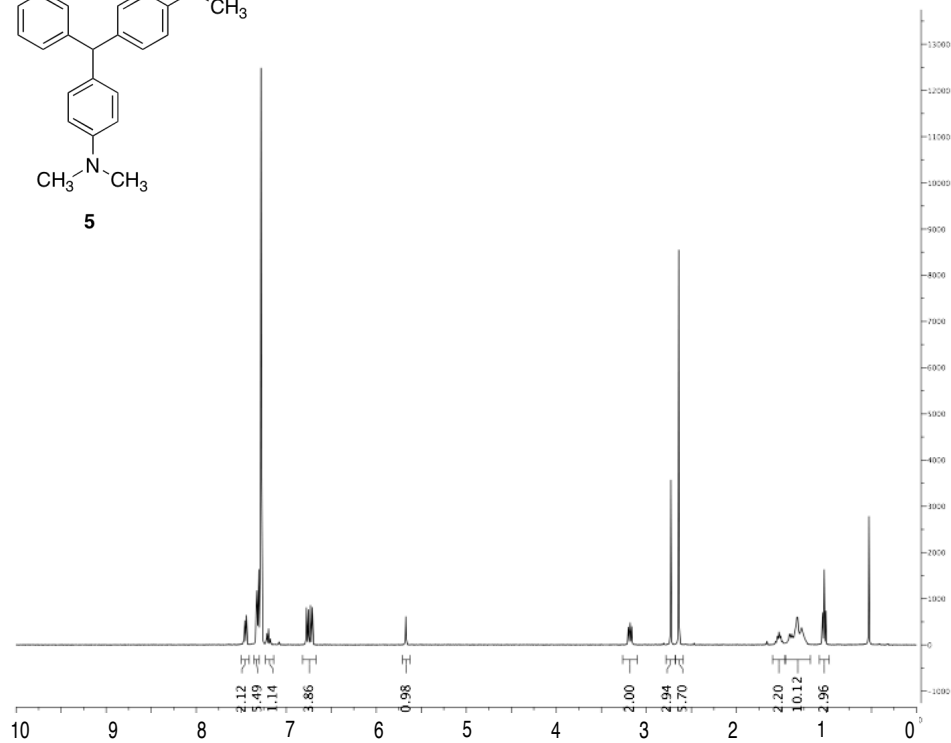
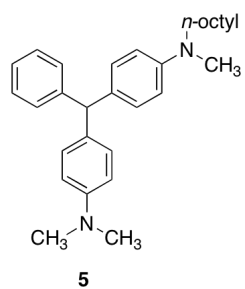
DEPT



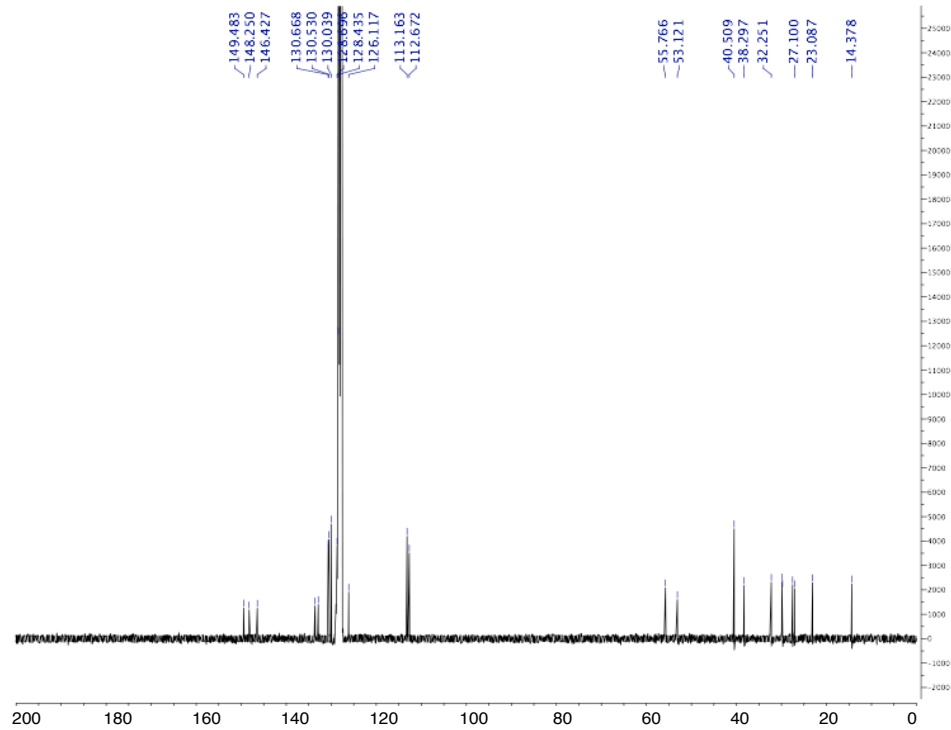
IR



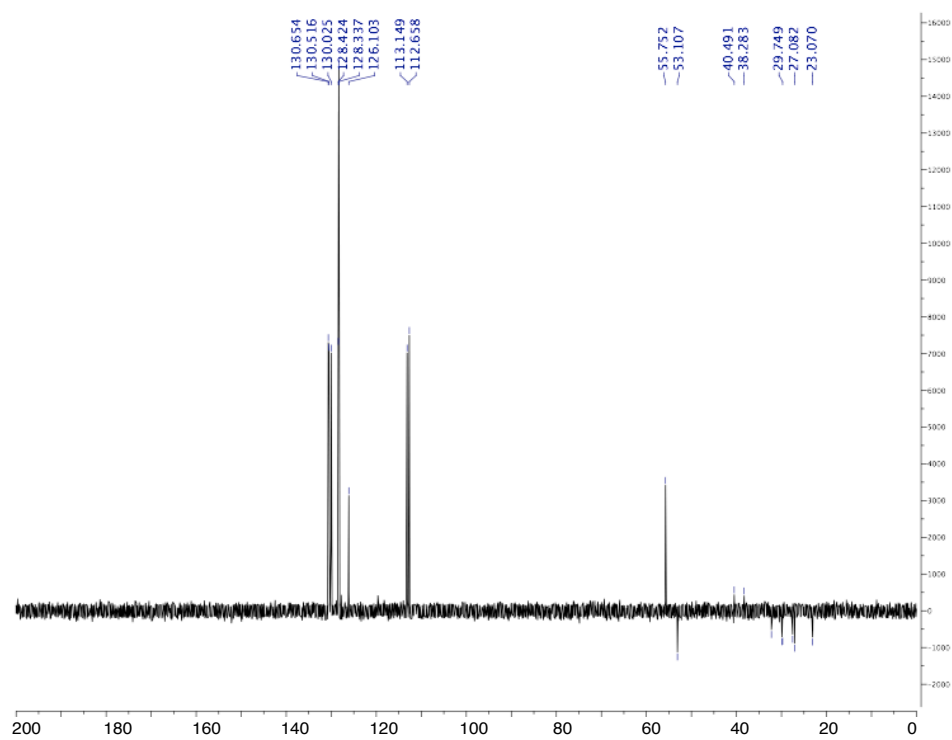
¹H NMR



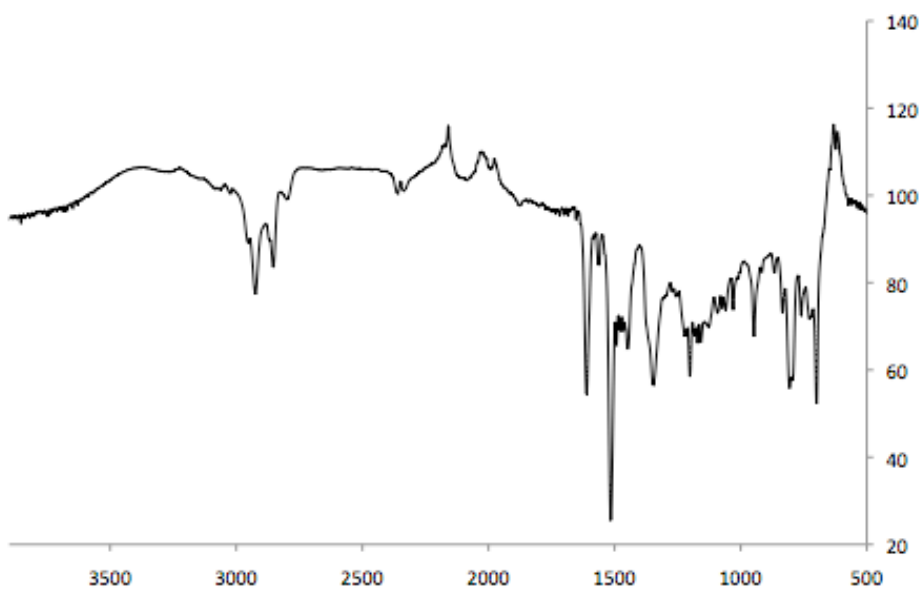
¹³C NMR



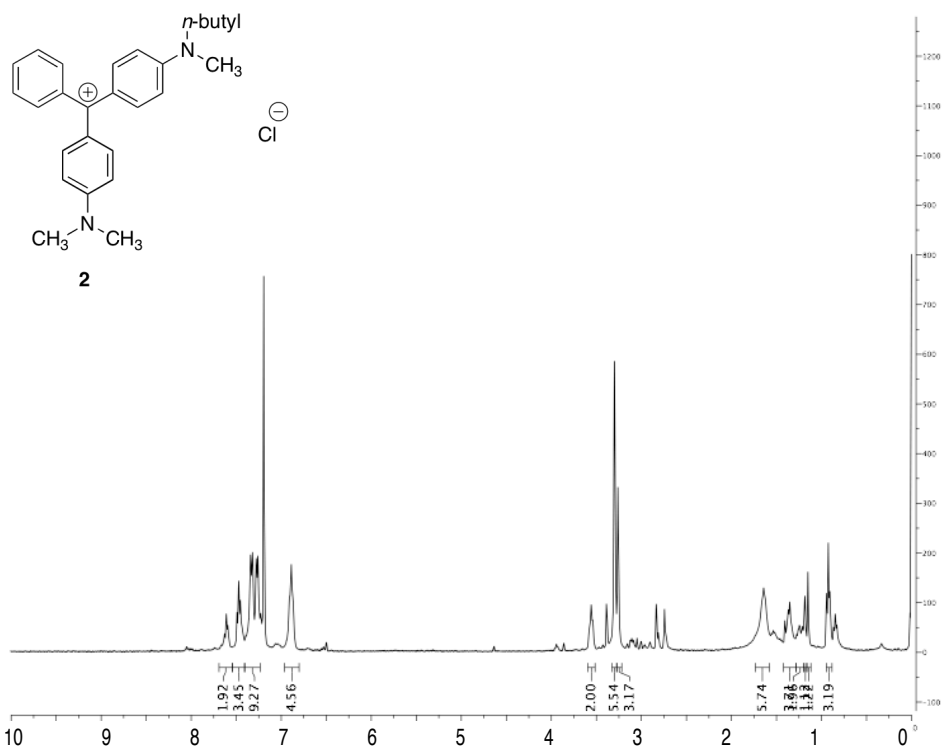
DEPT



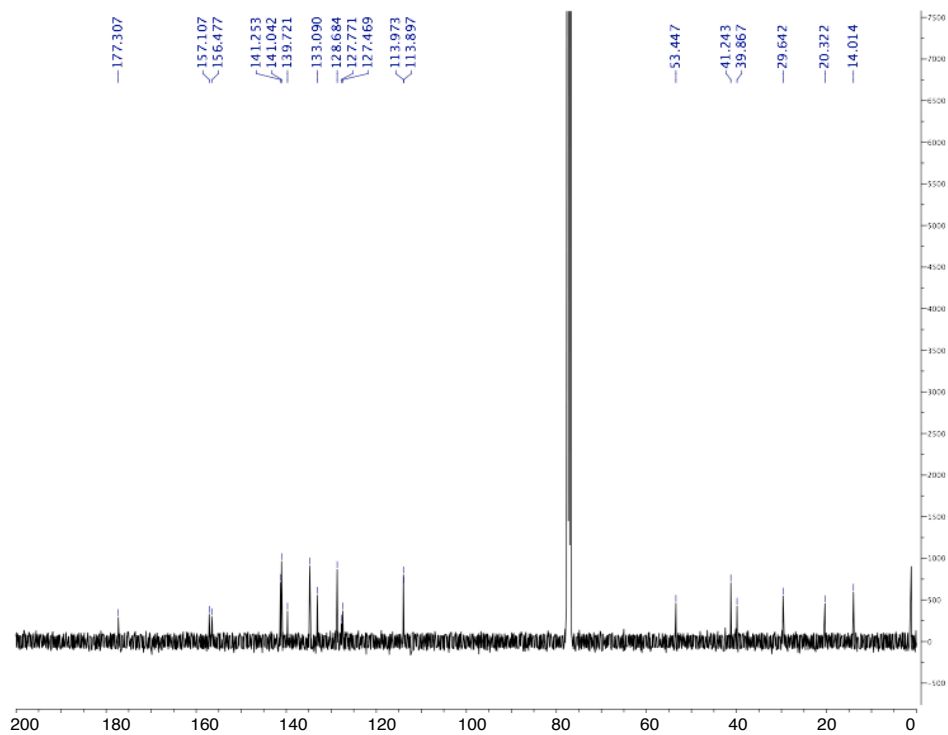
IR



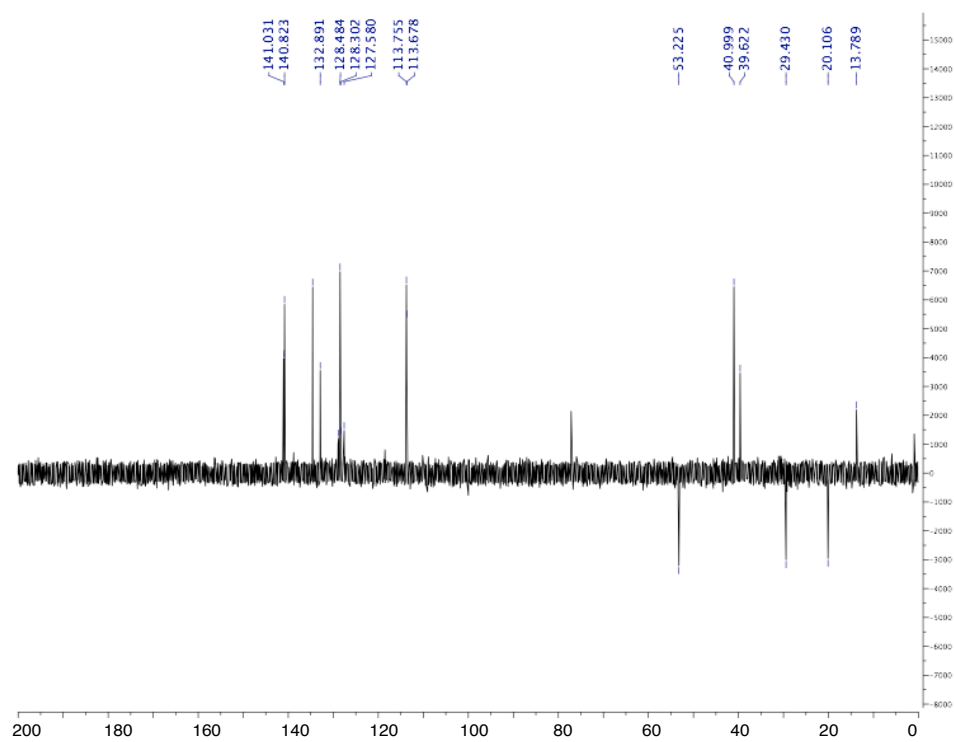
¹H NMR



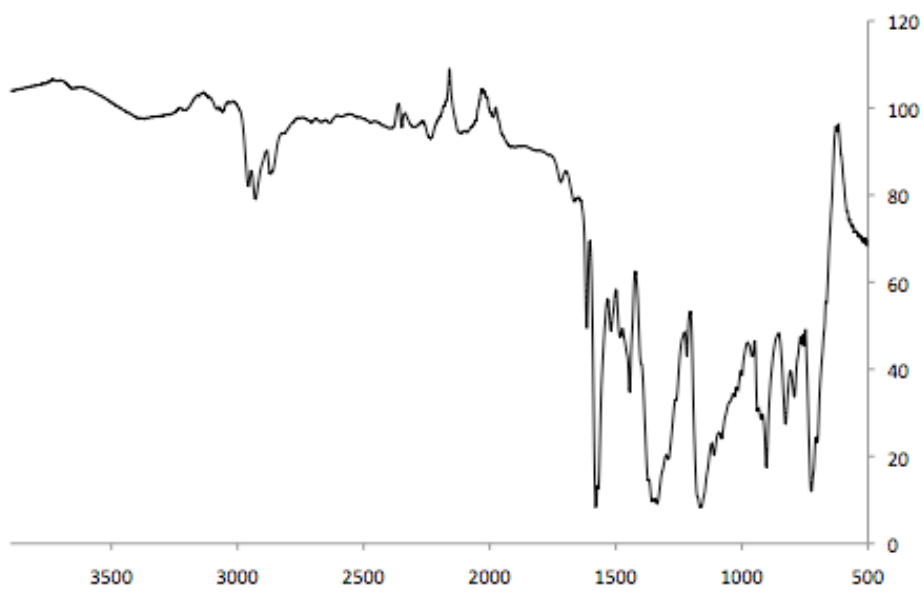
¹³C NMR



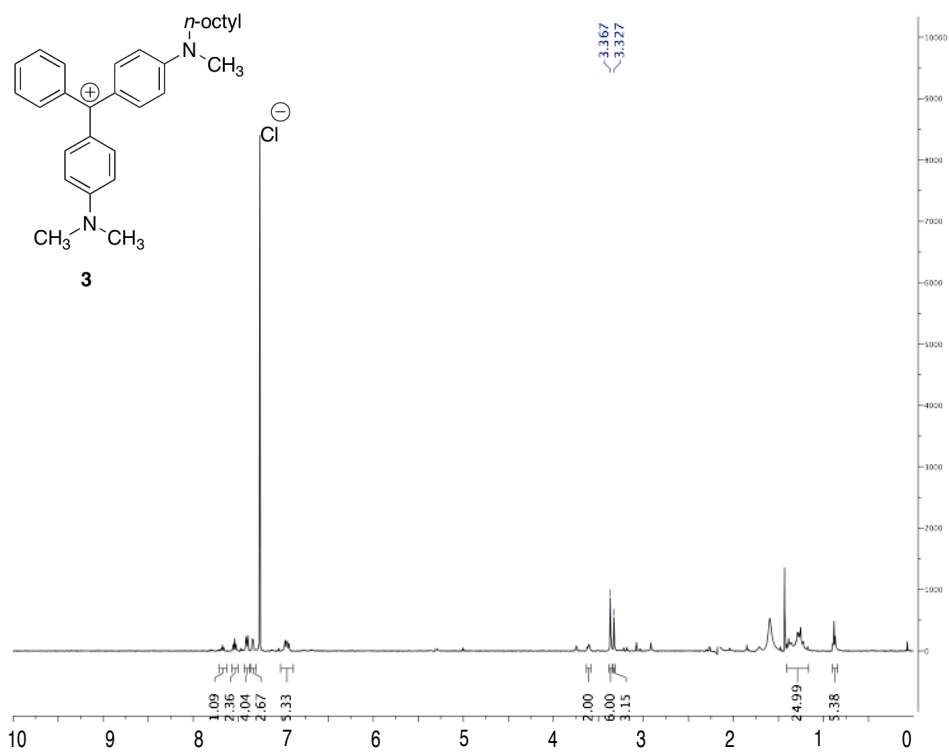
DEPT



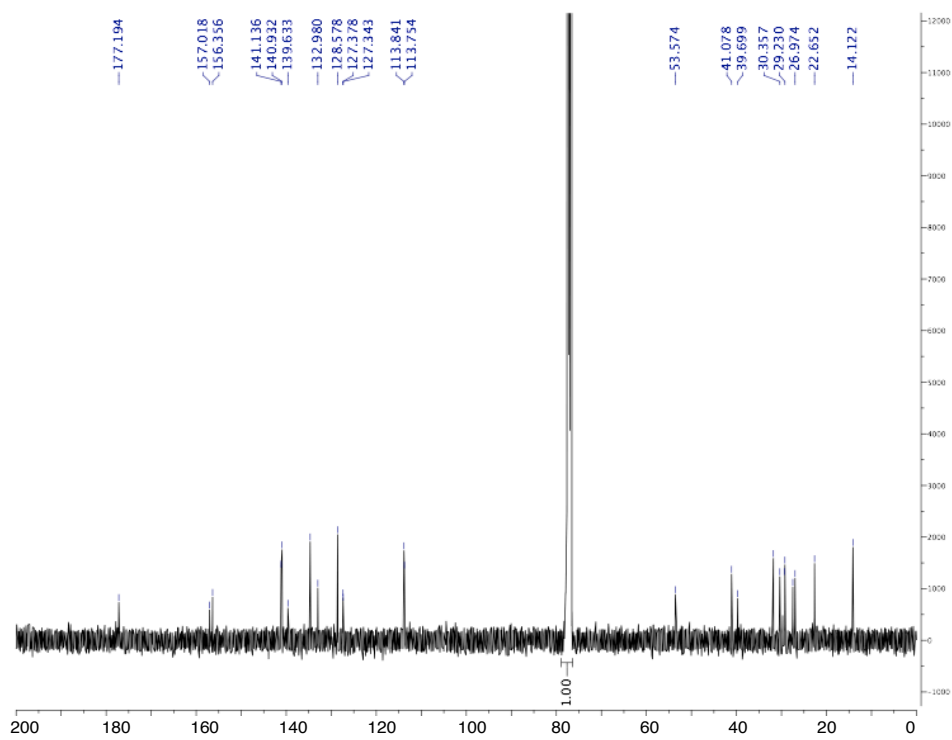
IR



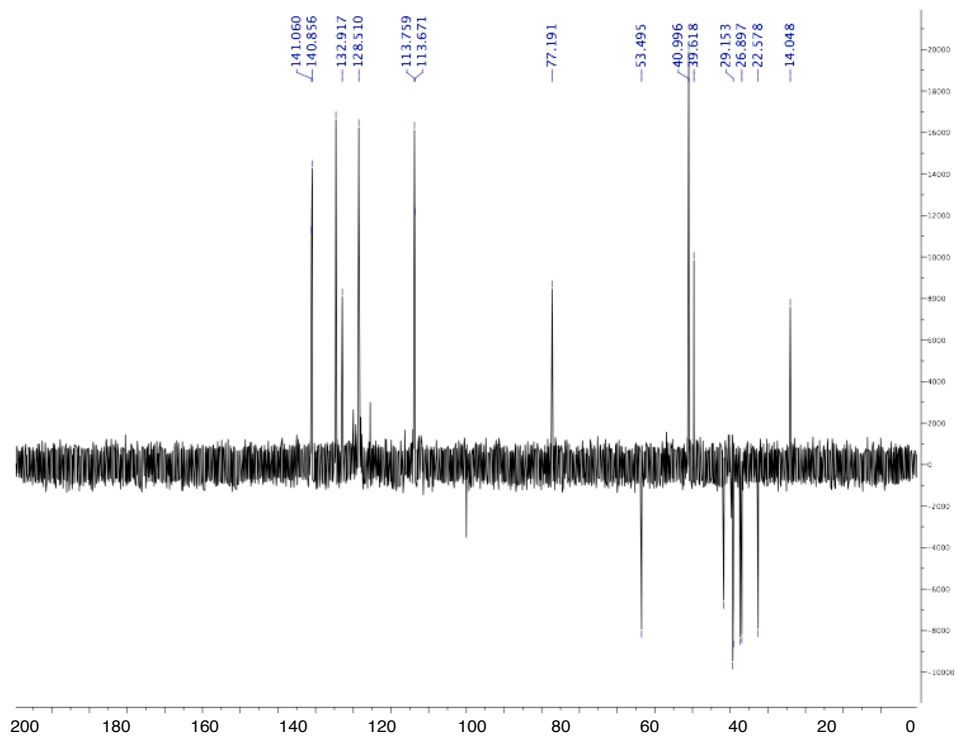
¹H NMR



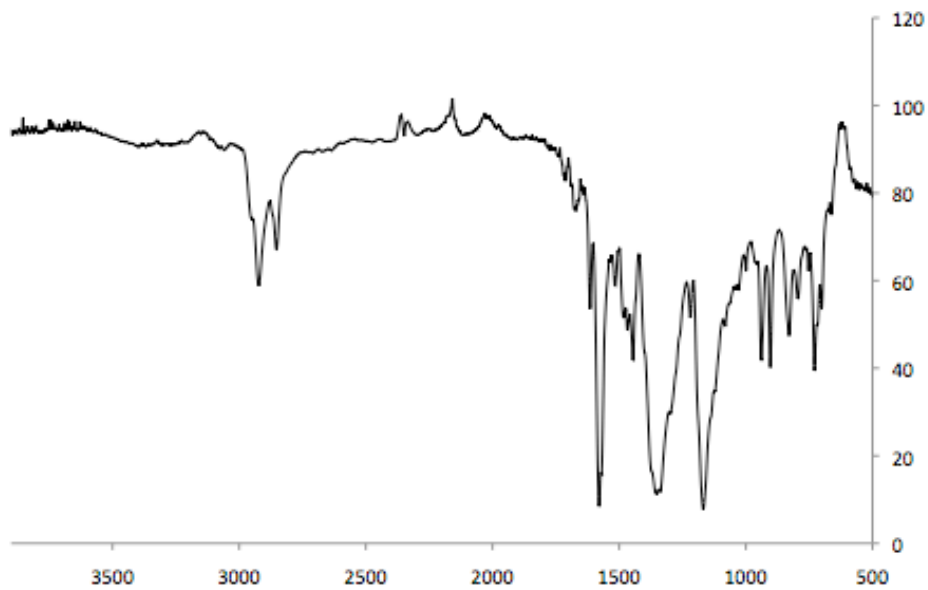
¹³C NMR



DEPT



IR



H. Theoretical Background of SHG: Probing Surfaces of Micron-Sized Colloidal Particles

Surface Specificity. The surface sensitivity of SHG spectroscopy originates from the selection rule that a second-order optical process is allowed under dipole approximation in non-centrosymmetric media but forbidden in centrosymmetric media.⁵⁻¹³ In the bulk, because asymmetric forces are absent, molecules are randomly oriented and centrosymmetry is preserved (Figure S4). On the other hand, molecules experience asymmetric forces across interfaces; thus, they are aligned and the centrosymmetry is broken. Consequently, the second-order polarization $P^{(2)}$ induced at non-centrosymmetric interfaces can add up coherently, which can be expressed as

$$E_{2\omega} \propto P^{(2)} \propto \chi^{(2)} E_{2\omega} E_{2\omega} \quad (\text{S2}),$$

where $E_{2\omega}$ is the second-harmonic (SH) field and $\chi^{(2)}$ is the second-order susceptibility. The macroscopic $\chi^{(2)}$ is related to the microscopic second-order polarizability $\alpha^{(2)}$ by

$$\chi^{(2)} = N \langle \alpha^{(2)} \rangle \quad (\text{S3}),$$

where N is the surface density of interfacial molecules and the bracket indicates an average over molecular orientation. The microscopic $\alpha^{(2)}$ is related to the transitions of interfacial molecules such that SHG signal can be enhanced when the fundamental frequency (ω) or the SH frequency (2ω) coincides with an electronic transition of the molecules (Figure S4).

Applications to Colloidal Surfaces. In the past decades, the SHG method has been extended to colloidal surfaces.^{2,3,14-34} Although a colloidal particle is centrosymmetric, molecules

are aligned at the interface and second harmonic field can still be generated locally at the interface (Figure S5). If the size of particles is sub-micron, the scale of wavelength, $E_{2\omega}$ generated at the surface of a particle can add up coherently to yield a finite SHG signal. This signal, accordingly to Equations (S2&S3), depends on N^2 . The idea of coherent addition of surface-specific second harmonic field generated from

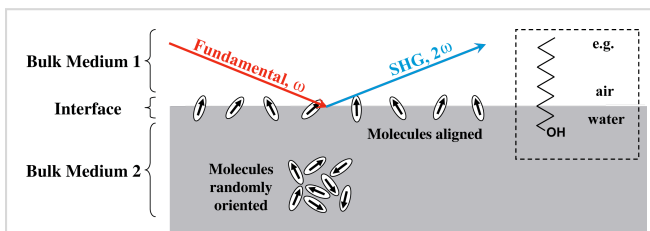


Figure S4. SHG is allowed in non-centrosymmetric interface but forbidden in centrosymmetric bulk medium.

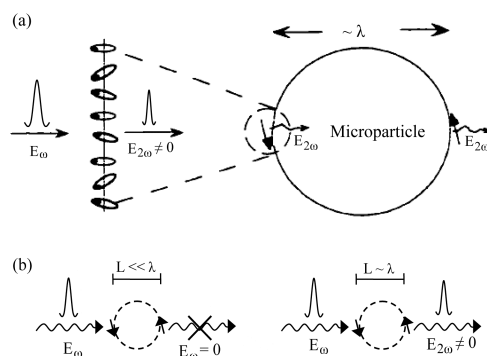


Figure S5. (a) Molecules are aligned at the surface of a particle. (b) Surface $E_{2\omega}$ depends on the size of the particle.

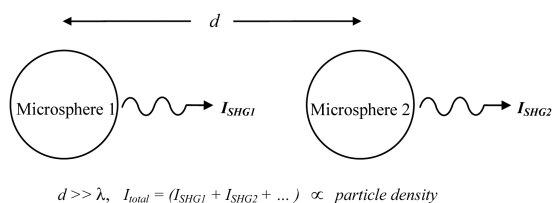


Figure S6. Incoherent addition of $E_{2\omega}$ from individual particles.

surfaces of microparticles has been implemented to study various colloidal systems including polymer particles,^{2,3,14-21} carbon black particles,²³ emulsions,^{3,15} clay particles,²⁴⁻²⁶ and liposomes²⁷⁻³³ to obtain surface information. In the past few years, another second-order optical method, sum frequency generation,^{7,9,35-39} which can probe vibrational structures, has also been applied to investigate the properties of particle surfaces.⁴⁰⁻⁴³

SHG—A Coherent Optical Method. Because of the coherent nature of the SHG optical process, the intensity (I_{SHG}) generated from micron-sized particles depends differently on surface population (N , number of molecules per unit area) and particle density (ρ , number of particles per unit volume).^{10,14} For $I_{SHG} = |E_{2\omega}|^2$, equations (S2-S3) require I_{SHG} generated from an individual particle to be directly proportional to N^2 . When the separation of the particles is much larger than the length scale of wavelength, $E_{2\omega}$ generated from different particles add up incoherently to give the total observed SHG intensity, $I_{SHG-total}$ (Figure S6).^{10,14} Hence, $I_{SHG-total} = (I_{SHG1} + I_{SHG2} + I_{SHG3} \dots + I_{SHGi} \dots)$, where I_{SHGi} ($\propto N^2$) is the SHG signal generated from particle i . Consequently, $I_{SHG-total}$ scales linearly with the product of ρ and N^2 , i.e., $I_{SHG-total} \propto \rho N^2$.

I. Experimental Evidence of the ρN^2 Dependence of I_{SHG}

We have analyzed our adsorption isotherm data and kinetic data in order to demonstrate that the ρN^2 dependence of I_{SHG} is valid for the emulsion system under study. First, the plot of I_{SHG} versus N on the logarithm scale can be obtained from the data presented in the adsorption isotherm (Figure S1), similar to the analyses reported by Wang *et al.*¹⁴ The particle density was fixed at 1.3×10^{10} particles/cm³, while the total concentration of Sp was varied. The low concentration region of the adsorption isotherm (Figure S1), where the surface population of Sp scales linearly with the total Sp concentration, is considered. Figure S7 shows the plot of I_{SHG} versus N on the logarithm scale, which gives a slope of 2.2 ± 0.2 . The result suggests a quadratic N^2 dependence of I_{SHG} . Second, from our kinetic data, as those presented in Figure 2 in the manuscript, we measured I_{SHG} at $t = 0$ upon dilution of the donor particle solution with the acceptor particle solution. Since different dilution factors can lead to different donor particle density at $t = 0$, the dependence of I_{SHG} on particle density (ρ) can be revealed. Figure S8 presents the plot of I_{SHG} versus ρ on the logarithm scale. The plot shows a slope of 1.01 ± 0.05 , suggesting that I_{SHG} depends linearly on ρ .

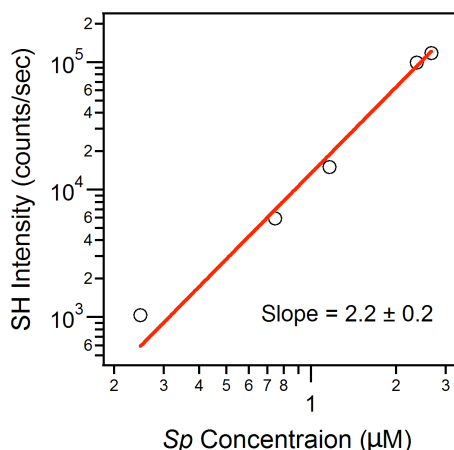


Figure S7. The plot of SHG intensity (I_{SHG}) versus surface population (N).

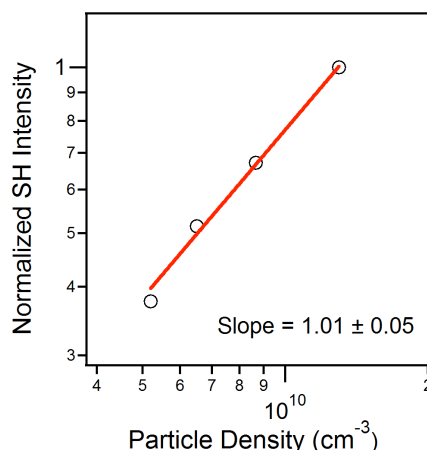


Figure S8. The plot of SHG intensity (I_{SHG}) versus particle density (ρ).

Moreover, we measured I_{SHG} at equilibrium conditions by fixing MG concentration at $2.3 \mu\text{M}$ and varying particle density from 1.30×10^{10} to 5.20×10^{10} particles/ cm^3 . Under these conditions, our adsorption isotherm data suggest that all MG molecules adsorb onto the emulsion particles. Hence, the numerical values of ρN^2 can be calculated, as shown in Table S1. Subsequently, I_{SHG} versus ρN^2 can be plotted on the logarithm scale (Figure S9). The slope of the plot is 1.2 ± 0.1 . This result, in conjunction with the results presented in Figure S7 and S8, has demonstrated that I_{SHG} depends linearly on ρN^2 . Thus, the ρN^2 dependence is valid for the emulsion system used in our studies.

Table S1 The ρN^2 dependence of SHG intensity.

| Particle Density ρ (cm^{-3}) | MG per particle N | $N^2\rho$ | SHG Intensity (counts/sec) |
|--|---------------------|-----------------------|----------------------------|
| 1.30×10^{10} | 106508 | 1.47×10^{20} | 20202 ± 721 |
| 1.70×10^{10} | 81447 | 1.13×10^{20} | 15227 ± 330 |
| 2.60×10^{10} | 53254 | 7.37×10^{19} | 8219 ± 625 |
| 5.20×10^{10} | 26627 | 3.69×10^{19} | 3588 ± 223 |

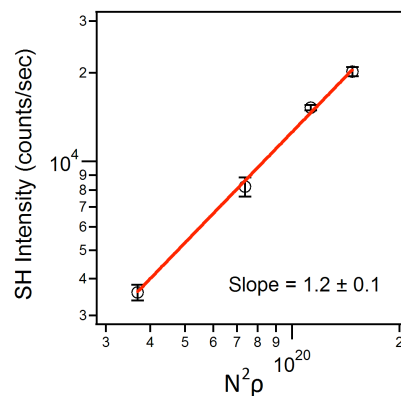


Figure S9. The SHG intensity is plotted a function of ρN^2 .

References:

- (1) Still, W. C.; Kahn, M.; Mitra, A. *J. Org. Chem.* **1978**, *43*, 2923-2925.
- (2) Wang, H. F.; Troxler, T.; Yeh, A. G.; Dai, H. L. *Langmuir* **2000**, *16*, 2475-2481.
- (3) Wang, H. F.; Yan, E. C. Y.; Liu, Y.; Eienthal, K. B. *J. Phys. Chem. B* **1998**, *102*, 4446-4450.
- (4) Schwarzenbach, R. P.; Gschwend, P. M.; Imboden, D. M. *Environmental organic chemistry*; Second ed.; John Wiley & Sons: Hoboken, New Jersey, 2003.
- (5) Bloembergen, N.; Pershan, P. *Phys. Rev.* **1962**, *128*, 606-622.
- (6) Shen, Y. R. *The principles of Nonlinear Optics*; Wiley: New York, 1984.
- (7) Shen, Y. R. *Nature* **1989**, *337*, 519-525.
- (8) Shen, Y. R. *Annu. Rev. Phys. Chem.* **1989**, *40*, 327-350.
- (9) Eienthal, K. B. *Chem. Rev.* **1996**, *96*, 1343-1360.
- (10) Eienthal, K. B. *Chem. Rev.* **2006**, *106*, 1462-1477.
- (11) Corn, R. M.; Higgins, D. A. *Chem. Rev.* **1994**, *94*, 107-125.
- (12) Richmond, G.; Robinson, J.; Shannon, V. *Prog. Surf. Sci.* **1988**, *28*, 1-70.
- (13) Geiger, F. M. *Annu. Rev. Phys. Chem.* **2009**, *60*, p 61-83.
- (14) Wang, H.; Yan, E. C. Y.; Borguet, E.; Eienthal, K. B. *Chem. Phys. Lett.* **1996**, *259*, 15-20.
- (15) Yan, E. C. Y.; Liu, Y.; Eienthal, K. B. *J. Phys. Chem. B* **1998**, *102*, 6331-6336.
- (16) Eckenrode, H. M.; Jen, S. H.; Han, J.; Yeh, A. G.; Dai, H. L. *J. Phys. Chem. B* **2005**, *109*, 4646-4653.
- (17) Eckenrode, H. M.; Dai, H. L. *Langmuir* **2004**, *20*, 9202-9209.
- (18) Yang, N.; Angerer, W.; Yodh, A. *Phys. Rev. Lett.* **2001**, *87*, 103902.
- (19) Schneider, L.; Schmid, H.; Peukert, W. *Appl. Phys. B-Lasers O.* **2007**, *87*, 333-339.
- (20) Campen, R. K.; Zheng, D. S.; Wang, H. F.; Borguet, E. *J. Phys. Chem. C* **2007**, *111*, 8805-8813.
- (21) Vidal, X.; Fedyanin, A.; Molinos-Gomez, A.; Rao, S.; Martorell, J.; Petrov, D. *Opt. Lett.* **2008**, *33*, 699-701.
- (22) Liu, Y.; Dadap, J. I.; Zimdars, D.; Eienthal, K. B. *J. Phys. Chem. B* **1999**, *103*, 2480-2486.
- (23) Wang, H. F.; Troxler, T.; Yeh, A. G.; Dai, H. L. *J. Phys. Chem. C* **2007**, *111*, 8708-8715.
- (24) Yan, E. C. Y.; Eienthal, K. B. *J. Phys. Chem. B* **1999**, *103*, 6056-6060.
- (25) Yan, E. C. Y.; Eienthal, K. B. *J. Phys. Chem. B* **2000**, *104*, 6686-6689.
- (26) Yan, E. C. Y.; Liu, Y.; Eienthal, K. B. *J. Phys. Chem. B* **2001**, *105*, 8531-8537.
- (27) Srivastava, A.; Eienthal, K. B. *Chem. Phys. Lett.* **1998**, *292*, 345-351.
- (28) Yan, E. C. Y.; Eienthal, K. B. *Biophys. J.* **2000**, *79*, 898-903.
- (29) Liu, Y.; Yan, C. Y.; Zhao, X. L.; Eienthal, K. B. *Langmuir* **2001**, *17*, 2063-2066.
- (30) Liu, Y.; Yan, E. C. Y.; Eienthal, K. B. *Biophys. J.* **2001**, *80*, 1004-1012.
- (31) Shang, X. M.; Liu, Y.; Yan, E.; Eienthal, K. B. *J. Phys. Chem. B* **2001**, *105*, 12816-12822.
- (32) Liu, J.; Shang, X. M.; Pompano, R.; Eienthal, K. B. *Faraday Discuss.* **2005**, *129*, 291-299.
- (33) Yamaguchi, A.; Nakano, M.; Nochi, K.; Yamashita, T.; Morita, K.; Teramae, N. *Anal. Bioanal. Chem.* **2006**, *386*, 627-632.
- (34) Sandrock, M. L.; Pibel, C. D.; Geiger, F. M.; Foss, C. A. *J. Phys. Chem. B* **1999**, *103*, 2668-2673.
- (35) Richmond, G. L. *Chem. Rev.* **2002**, *102*, 2693-2724.
- (36) Miranda, P. B.; Shen, Y. R. *J. Phys. Chem. B* **1999**, *103*, 3292-3307.
- (37) Stokes, G. Y.; Gibbs-Davis, J. M.; Boman, F. C.; Stepp, B. R.; Condie, A. G.; Nguyen, S. T.; Geiger, F. M. *J. Am. Chem. Soc.* **2007**, *129*, 7492-+.
- (38) Shultz, M. J.; Schnitzer, C.; Simonelli, D.; Baldelli, S. *Int. Rev. Phys. Chem.* **2000**, *19*, 123-153.
- (39) Liu, D. F.; Ma, G.; Levering, L. M.; Allen, H. C. *J. Phys. Chem. B* **2004**, *108*, 2252-2260.
- (40) Roke, S.; Roeterdink, W. G.; Wijnhoven, J.; Petukhov, A. V.; Kleyn, A. W.; Bonn, M. *Phys. Rev. Lett.* **2003**, *91*, 258302.
- (41) Roke, S.; Bonn, M.; Petukhov, A. V. *Phys. Rev. B* **2004**, *70*, 115106.
- (42) Roke, S. *Chemphyschem* **2009**, *10*, 1380-1388.
- (43) de Beer, A. G. F.; Roke, S. *Phys. Rev. B* **2007**, *75*, 245438.

